iScience

Article

# Ape-like locomotor adaptations in the radius of the stem catarrhine *Pliobates* shed light on hominoid evolution

## Graphical abstract

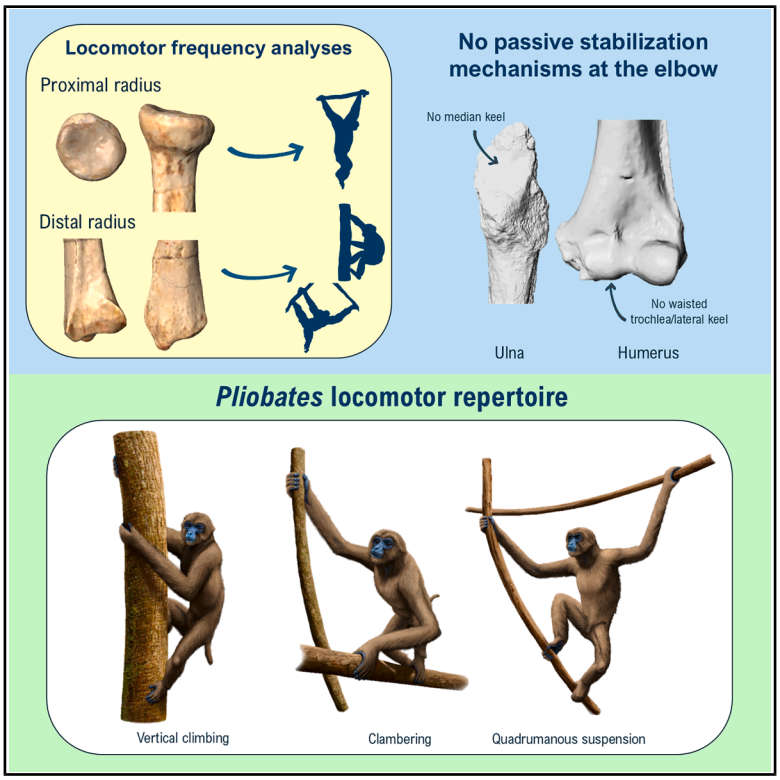


## Highlights

- The proximal radius of *Pliobates* is convergent with that of crown hominoids
- The *Pliobates* apelike proximal radius contrasts with its more primitive distal radius
- *Pliobates* illustrates the mosaic and stepwise evolution of the catarrhine forelimb
- The proximal radius of *Pliobates* is an adaptation for climbing instead of suspension

## Authors

Julia Arias-Martorell, Georgina Raventós-Izard, Oriol Monclús-Gonzalo, ..., Masato Nakatsukasa, Salvador Moyà-Solà, David M. Alba

## Correspondence

julia.arias@icp.cat

## In brief

Natural sciences; Evolutionary biology; Paleobiology

Arias-Martorell et al., 2026, iScience *29*, 114622
February 20, 2026 
https://doi.org/10.1016/j.isci.2025.114622

CellPress

iScience

CellPress
OPEN ACCESS

Article

# Ape-like locomotor adaptations in the radius of the stem catarrhine *Pliobates* shed light on hominoid evolution

Julia Arias-Martorell,[1,8,*] Georgina Raventós-Izard,[1] Oriol Monclús-Gonzalo,[1] Alessandro Urciuoli,[1,2,3,4] Jesús Gamarra,[1] Masato Nakatsukasa,[5] Salvador Moyà-Solà,[1,6] and David M. Alba[1,7]

[1]Institut Català de Paleontologia Miquel Crusafont (ICP-CERCA), Universitat Autònoma de Barcelona, Cerdanyola del Vallès, Barcelona 08193, Spain
[2]Department of Paleontology, University of Zurich, Zürich 8006, Switzerland
[3]Division of Palaeoanthropology, Senckenberg Research Institute and Natural History Museum Frankfurt, Frankfurt am Main 60325, Germany
[4]Universidad de Alcalá, Cátedra de Otoacústica Evolutiva y Paleoantropología (HM Hospitales-UAH), Departamento de Ciencias de la Vida, Alcalá de Henares, Madrid 28871, Spain
[5]Laboratory of Physical Anthropology, Graduate School of Science, Kyoto University, Kyoto 606-8502, Japan
[6]Unitat d'Antropologia Biològica (Departament de Biologia Animal, de Biologia Vegetal i d'Ecologia), Universitat Autònoma de Barcelona, Cerdanyola del Vallès, Barcelona 08193, Spain
[7]Senior author
[8]Lead contact
*Correspondence: julia.arias@icp.cat
https://doi.org/10.1016/j.isci.2025.114622

## SUMMARY

The 11.6. Ma pliopithecoid *Pliobates* was initially misinterpreted as a stem hominoid owing to multiple apelike postcranial features. Using 3D geometric morphometrics, we compare its radial shape with that of extant and extinct catarrhines to make locomotor inferences. The round and beveled radial head of *Pliobates* resembles that of modern apes, which we interpret as functionally related to efficient forearm rotation. This contrasts with its more plesiomorphic distal radius and proximal ulna, suggesting that *Pliobates* was more adapted for climbing than forelimb-dominated suspension and unable to perform gibbon-like ricochetal brachiation. Our results illustrate the mosaic and stepwise evolution of the catarrhine elbow and support the view that an apelike proximal radial morphology evolved multiple times as a climbing rather than suspensory adaptation. This agrees with the possibility that several features of the hominoid elbow were originally selected for climbing and subsequently co-opted for suspensory locomotion.

## INTRODUCTION

The small-bodied (~5 kg) catarrhine primate *Pliobates cataloniae*, from the Miocene (11.6 Ma) of Abocador de Can Mata (Vallès-Penedès Basin, NE Iberian Peninsula), is currently considered a crouzeliid pliopithecoid[1,2]—i.e., a stem catarrhine lineage whose origins precede the divergence between hominoids (apes and humans) and cercopithecoids (Old World monkeys).[3,4] *Pliobates* combines a diagnostic pliopithecoid dental morphology[1,2] with a mosaic of stem-catarrhine-like and modern-ape-like cranial and postcranial features.[1,5] Cladistic analyses originally recovered *Pliobates* as a stem hominoid[5] and subsequently supported it as a pliopithecoid and/or a stem catarrhine.[6–8] Most recently, it has been shown that cladistic analyses only recover *Pliobates* and other pliopithecoids as stem hominoids when postcranial data are included.[1] This is due to multiple convergences with crown hominoids, which on qualitative grounds are most clearly evinced in the humeroradial and diarthrodial distal radioulnar joints.[1,5] These postcranial features are functionally related to locomotion,[9–13] which might explain their independent evolution in various groups.

The problem of pervasive homoplasy—i.e., the independent acquisition of similar features, due to convergence—in the hominoid locomotor apparatus has long been noted.[14] Nevertheless, some authors have interpreted the acquisition of the orthograde body plan—characteristic of all extant hominoids and functionally related to antipronograde behaviors with an upright torso[15–18]—as an adaptation for below-branch, forelimb-dominated suspensory behaviors, purportedly synapomorphic of either hominoids[19–21] or hominids (great apes and humans).[22] However, this is not supported by fossil evidence, given the postcranial morphology of Miocene apes such as *Pierolapithecus*[23,24] and *Sivapithecus*,[25,26] more plesiomorphic than expected based on the synapomorphies shared by their modern counterparts,[27,28] or that of *Oreopithecus*, more derived than expected based on its likely stem hominoid status.[29] The presence of some orthograde features in other extant taxa such as atelids,[30] along with the differences in forelimb morphology among extant apes,[10,11,30] further supports this view. Recent authors have thus highlighted the contradictory phylogenetic signal provided by craniodental vs. postcranial morphology in apes,[1,28,31]


**Figure 1. Photographs of the original specimen: the left radius of *Pliobates cataloniae***

(A) Posterior view, (B) lateral view, (C) anterior view, (D) medial view, (E) proximal view, and (F) distal view.

supporting the view that suspensory adaptations might have independently evolved along various ape lineages from an ancestral condition emphasizing climbing but not suspension[23,24,27–29]—as previously hypothesized by some authors for the ancestral hominoid condition.[32,33]

*Pliobates*—as a stem catarrhine convergent with hominoids in key anatomical features of the elbow and wrist[1,5,13]—provides a unique opportunity to evaluate the degree of postcranial convergence among different catarrhine lineages in detail. At the same time, *Pliobates* has been inferred to be a cautious climber with a restricted and non-acrobatic suspensory component,[5,13] thus potentially providing insight into the plausibility of a non-suspensory but climbing ancestral stage preceding the divergence of extant, suspensory ape lineages. With these aims in mind, here we offer a detailed description of the radius of *Pliobates* and quantitatively compare the shape of its proximal and distal epiphyses with that of other taxa by means of 3D geometric morphometrics (3DGM). On this basis, we also estimate the locomotor repertoire of *Pliobates* using a locomotor frequency analysis via a partial least-squares regression (PLSR) approach. The implications for the emergence of extant hominoid locomotor specializations are discussed.

## RESULTS

### Description

The complete left radius of *Pliobates* (Figure 1) is long and slender overall, with a slight curvature of the shaft in the mediolateral plane, being overall quite straight. The preservation of the shaft is poorer than that of the epiphyses, with cortical bone broken off in some parts and being abraded at midshaft. The radial head exhibits no mediolateral tilting, but the posteromedial portion of the head is slightly elevated over the rest of the articular surface. The latter is round and exhibits a beveled surface that extends all around the radial head, with a wide fovea that occupies most of the proximal articular surface and is centrally positioned. The articular surface extends distally, being widest in its anteromedial portion, toward the radial neck. The latter is relatively long, flattened mediolaterally, and anteroposteriorly wide. The radial tuberosity is oriented medially, with well-defined margins. The distal epiphysis is moderately narrow mediolaterally, and the radial styloid is well defined and protrudes distally. The dorsal tubercle is slightly prominent, being most defined in its distalmost portion. The ulnar notch is wide and flattened, and the articular facets of the lunate and the scaphoid are similarly sized; the lunate facet is at a marked angle from the scaphoid facet.

### 3D geometric morphometrics

The 3DGM analysis of the whole radius (Figures S1 and S2; Data S1) chiefly distinguishes long and slender from short and robust radii. Comparatively, the finer details of the articular morphology—which has functional implications regarding locomotion—have a diminished influence. Hence, we focus below on the separate results for the proximal and distal epiphyses.

None of the between-group principal components (bgPCs) considered for the proximal and distal datasets are correlated with ln CS (Table S1). The between-group principal-component analysis (bgPCA) for the proximal radius correctly classifies 74% specimens (71% for the cv-bgPCA) into the *a priori* defined groups (hominoids, cercopithecoids, platyrrhines, and lorisids). The bgPC1 (57% of variance; Figure 2) embeds significant ($p < 0.001$) phylogenetic signal with and without fossils, with $K$ values being considerably lower (from $K = 0.81$ to $K = 0.41$, respectively; Table S2) when fossils are included in the analysis. This axis separates hominoids (hominids and hylobatids) and lorisids (on negative values) from the other groups (on positive bgPC1 scores), except for an overlap between some cercopithecoids (particularly *Mandrillus*) and the platyrrhine *Ateles*. Shape changes along bgPC1 (Figure 2) are driven by the tilting of the radial head, the wider and more centered fovea, and the absence of bevel on the posterior and lateral aspects of the radial head toward positive scores. The bgPC2 (27% of variance; Figure 2) embeds significant ($p < 0.001$) phylogenetic signal (with and without fossils) with low $K$ values (Table S2). This axis separates lorisids (overlapping with some *Pongo* specimens and *Ateles* on positive scores) from cercopithecoids (negative scores). The bgPC2 shape changes (Figure 2) are driven by the rounder radial head without tilting and the more anteriorly placed radial tuberosity

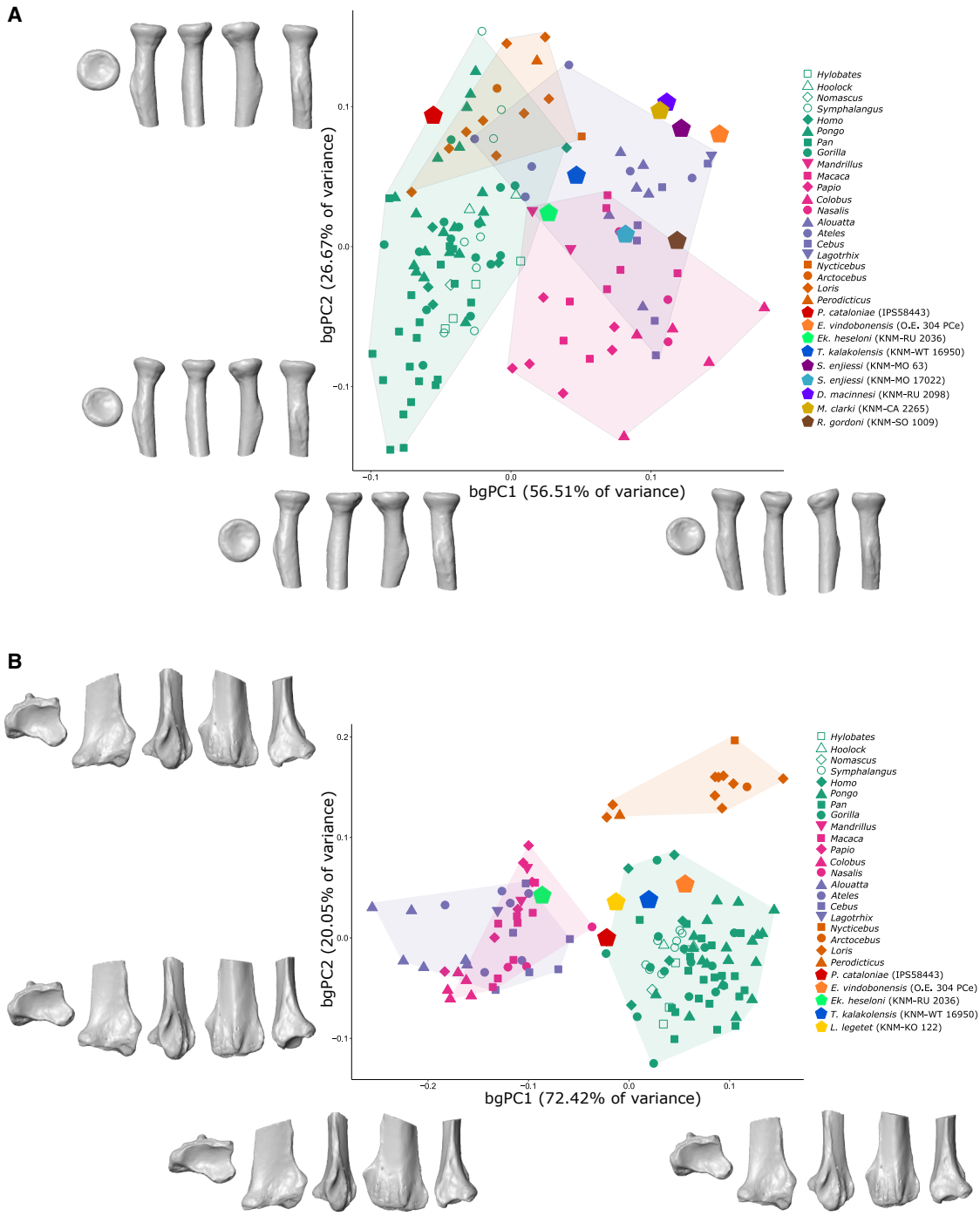


**Figure 2. Proximal and radius bgPC plot results**

Groups are color- and symbol-coded: hominoids are in green (hominids in filled symbols, hylobatids in outlines); platyrrhines in purple; cercopithecoids in pink; and lorisids in orange. Fossil specimens are denoted by colored pentagons. For the proximal radius, shape changes extracted from extreme configurations of each bgPC axis are warped onto a 3D model of a left proximal radius of a hylobatid (*Hylobates agilis*, AMNH 106575) in proximal, anterior, lateral, posterior, and medial views. For the distal radius, shape changes are warped onto a 3D model of a left distal radius of a chimpanzee (*Pan troglodytes* USNM 220063) in distal, anterior, lateral, posterior, and medial views.

(A) Bivariate plot of bgPC2 vs. bgPC1 depicting the results of the between-group principal-component analysis conducted on the proximal radial shape.

(B) Bivariate plot of bgPC2 vs. bgPC1 depicting the results of the between-group principal-component analysis conducted on the distal radial shape.

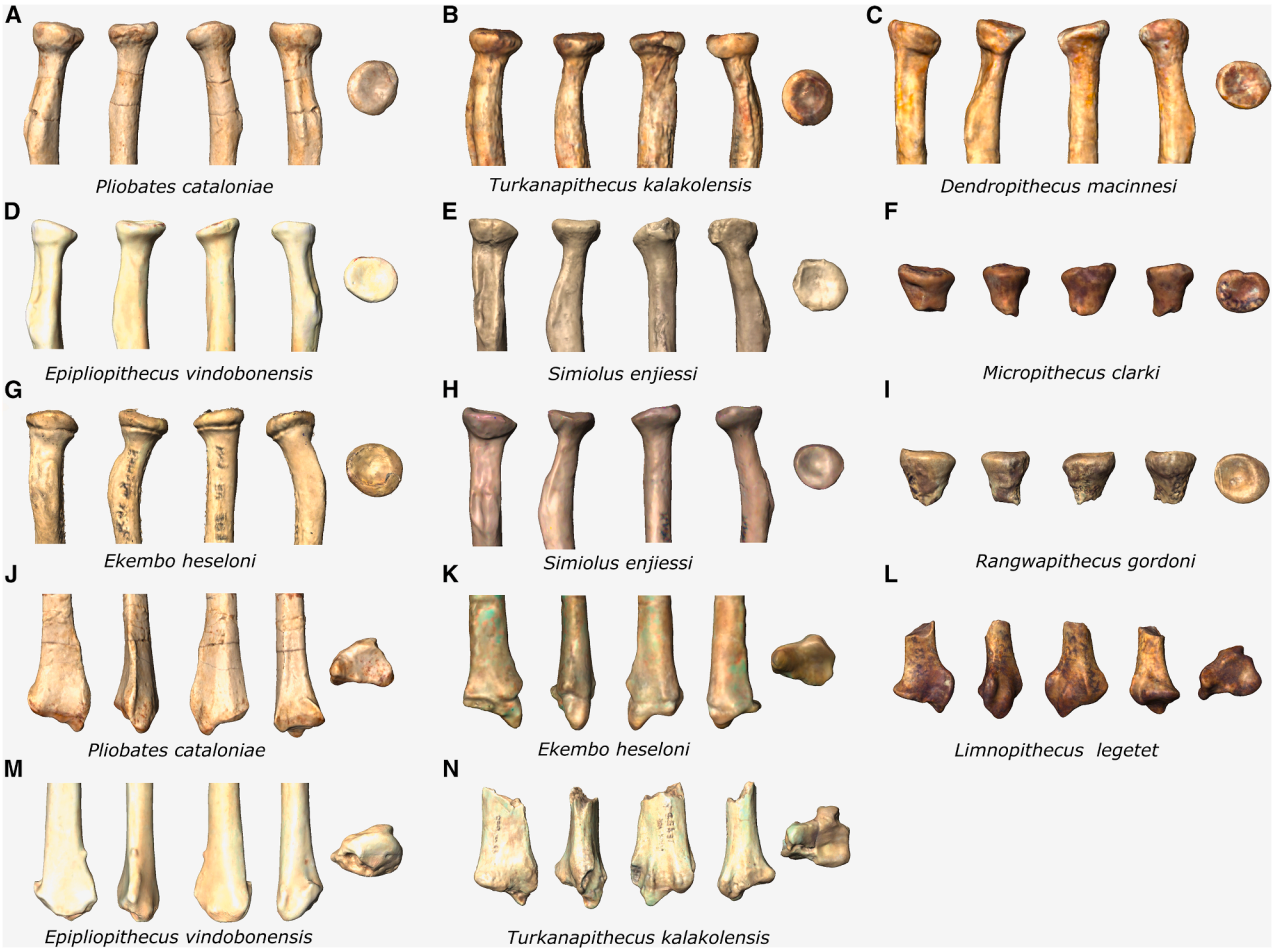


**Figure 3. Proximal and radial shape of fossils included in the analysis**

Rendered models of the fossils scanned and included in the analyses. The fossils included have the following catalog numbers:
(A and J) *P. cataloniae* (IPS58443.16).
(B and N) *Turkanapithecus kalakolensis* (KNM-WT 16950).
(C) *Dendropithecus macinnesi* (KNM-RU 2098).
(D and M) *Epipliopithecus vindobonensis* (O.E. 304 PCe).
(E) *Simiolus enjiessi* (KNM-MO 17022B).
(F) *Micrurus clarki* (KNM-CA 2265).
(G and K) *Ekembo heseloni* (KNM-RU 2036).
(H) *S. enjiessi* (KNM-MO 63).
(I) cf. *Rangwapithecus gordoni* (KNM-SO 1009).
(L) *Limnopithecus legetet* (KNM-KO 122).
(A–I) Fossils included in the proximal analyses in anterior, lateral, posterior, and medial, as well as a proximal view of the radial head.
(J–N) Fossils included in the distal analyses, in a distal view of the distal epiphysis of the radius.

toward positive scores. The proximal radius of *Pliobates* (round, without tilting, and with a wide fovea) is thus clearly ape-like and distinct from that of other extinct catarrhines (Figures 2 and 3), which approach platyrrhines and in some cases further overlap with cercopithecoids.

The bgPCA for the distal radius correctly classifies 95% specimens (94% for the cv-bgPCA). The bgPC1 (72% of variance; Figure 2) embeds significant ($p < 0.001$) phylogenetic signal (with and without fossils) with high $K$ values ($K = 1.63$ and 1.25, respectively; Table S2). This axis separates hominoids and lorisids (positive values) from cercopithecoids and platyrrhines (negative values). Shape changes along this axis (Figure 2) are related to the radial styloid, the size of the facet for the lunate relative to the scaphoid, and the size of the ulnar notch (larger and wider toward positive values). The bgPC2 (20% of variance; Figure 2) embeds significant ($p < 0.001$) phylogenetic signal with and without fossils, although $K$ values are considerably lower when fossils are included ($K = 0.87$ and 0.42, respectively; Table S2). This axis separates lorisids (positive values) from the rest. Shape changes along bgPC2 (Figure 2) are related to a relatively large lunate facet and a mediolaterally narrow epiphysis (positive values). When the two axes are considered, *Pliobates*

**Table 1. Posterior and typicality probabilities derived from the canonical variate analyses for extinct species**

| Species | Cercopithecoids | | Hominoids | | Lorisids | | Platyrrhines | |
|---|---|---|---|---|---|---|---|---|
| Proximal radius: | P | T | P | T | P | T | P | T |
| *Pliobates cataloniae* (IPS58443) | 0% | <0.001 | **92%** | **0.129** | 8% | 0.014 | 0% | <0.001 |
| *Epipliopithecus vindobonensis* (O.E. 304 PCe) | 0% | <0.001 | 0% | <0.001 | 0% | <0.001 | **100%** | **0.005** |
| *Simiolus enjiessi* (KNM-MO 17022B) | 5% | 0.109 | 0% | <0.001 | 0% | <0.001 | **95%** | **0.984** |
| *Simiolus enjiessi* (KNM-MO 63) | 0% | <0.001 | 0% | <0.001 | 0% | <0.001 | **100%** | **0.055** |
| *Micropithecus clarki* (KNM-CA 2265) | 0% | <0.001 | 0% | <0.001 | 1% | <0.001 | **99%** | **0.120** |
| *Dendropithecus macinnesi* (KNM-RU 2098) | 0% | <0.001 | 0% | <0.001 | 1% | <0.001 | **99%** | **0.341** |
| *Ekembo heseloni* (KNM-RU 2036) | 20% | 0.098 | 24% | 0.114 | 15% | 0.077 | **42%** | **0.187** |
| *Turkanapithecus kalakolensis* (KNM-WT 16950) | 4% | 0.018 | 18% | 0.069 | 0% | <0.001 | **78%** | **0.249** |
| cf. *Rangwapithecus gordoni* (KNM-SO 1009) | 10% | 0.077 | 0% | <0.001 | 0% | <0.001 | **90%** | **0.249** |
| **Species** | **Cercopithecoids** | | **Hominoids** | | **Lorisids** | | **Platyrrhines** | |
| **Distal radius:** | **P** | **T** | **P** | **T** | **P** | **T** | **P** | **T** |
| *Pliobates cataloniae* (IPS58443) | 13% | 0.030 | **76%** | **0.144** | 1% | 0.003 | 10% | 0.024 |
| *Epipliopithecus vindobonensis* (O.E. 304 PCe) | 0% | <0.001 | 33% | 0.102 | **67%** | **0.185** | 0% | <0.001 |
| *Ekembo heseloni* (KNM-RU 2036) | 43% | 0.252 | 1% | 0.005 | 0% | 0.001 | **56%** | **0.311** |
| *Turkanapithecus kalakolensis* (KNM-WT 16950) | 0% | <0.001 | **73%** | **0.325** | 27% | 0.140 | 0% | 0.001 |
| *Limnopithecus legetet* (KNM-MO 122) | 7% | 0.017 | **78%** | **0.152** | 13% | 0.031 | 3% | 0.001 |
| **Species** | **Cercopithecoids** | | **Hominoids** | | **Lorisids** | | **Platyrrhines** | |
| **Whole radius:** | **P** | **T** | **P** | **T** | **P** | **T** | **P** | **T** |
| *Pliobates cataloniae* (IPS58443) | 0% | <0.001 | 0% | 0.002 | 0% | <0.001 | **100%** | **0.806** |
| *Epipliopithecus vindobonensis* (O.E. 304 PCe) | 0% | <0.001 | **100%** | **0.719** | 0% | 0.004 | 0% | <0.001 |

Both the posterior (P) and typicality (T) probabilities were derived for the proximal, distal, and complete radius datasets. Highest probabilities of group classification are bolded. Posterior probabilities are expressed in percentages (0%–100%) and add to 100% for all groups; in contrast, typicality probabilities denote the probability of belonging to each group separately (group membership rejected when $p < 0.05$).

occupies an intermediate position between cercopithecoids and platyrrhines on the one hand and hominoids and lorisids on the other. Despite being close to other extinct taxa (particularly, *Limnopithecus* and *Turkanapithecus*) that fall within the hominoid distribution (Figure 2), *Pliobates* is not far from *Ekembo* (which overlaps with cercopithecoids and closely approaches platyrrhines). The distal radius of *Pliobates* resembles that of apes in ulnar notch morphology but is overall less ape-like than the proximal epiphysis, with a relatively smaller lunate facet and thus more similarly sized lunar-scaphoid facets (Figures 2 and 3).

Group differences are significant at $p < 0.001$ for both the proximal and distal datasets, including the raw shape coordinates, the bgPCA, and the cv-bgPCA. Z scores and $R^2$ values (Table S3) are very similar in the bgPCA and the cv-bgPCA for all datasets (proximal and distal). Group differences accounted for 22%–30% of the variance in the bgPCA, cv-bgPCA, and for all shape (landmark coordinates after GPA), indicating that bgPCA grouping structure is not spurious—as further confirmed by standard PCAs without *a priori* defined groups (Figures S3 and S4; Data S1).

The CVA for the whole radius classifies 95% individuals into the *a priori* groups (93% after cross-validation; Figure S5). The CVA of the proximal radius correctly classifies 90% extant individuals (82% after cross-validation; Figure S6), whereas for the distal radius it correctly classifies 96% individuals (94% after cross-validation; Figure S7). Posterior probabilities (Table 1) classify *Pliobates* as a hominoid for both the proximal radius (92%) and the distal radius (76%), but it is classified as a platyrrhine for the whole radius (100%). Typicality probabilities for *Pliobates* indicate it is an outlier with respect to the morphological variability of all *a priori* groups except hominoids for the proximal and distal radius (Table 1). Other extinct taxa are generally classified as platyrrhines for both the proximal and the distal radius, except for *Turkanapithecus* and *Limnopithecus*, which are classified as hominoids for the proximal radius (Table 1). It is also noteworthy that *Ekembo* also fits well with the variation of other groups (particularly cercopithecoids for both the proximal and distal radius), as it is also the case of the proximal radius of *Turkanapithecus*.

## Locomotor frequency analysis

The PLSR tends to overestimate some locomotor behaviors (particularly quadrupedalism) in the predictions when all the sample (excluding humans) is used, accumulating error in the locomotor frequencies of quadrupedalism and clambering (Table S4), due to the inclusion of African apes (Figure S8; Data S1). When the analyses are conducted without African apes, error values are lower for all types (especially for quadrupedalism; Table S4). Therefore, results are given for the PLSR conducted without African apes.

For the proximal radius, there is significant covariation between the shape of the proximal radius and locomotion in the two first PLS axes, accounting for 94% of the total covariance (Figure 4; Table S5). In PLS1 (70% of covariance), hylobatids fall at the negative end, followed by *Pongo* (particularly *Pongo pygmaeus*) and, with more intermediate values, *Ateles* and lorisids. At the

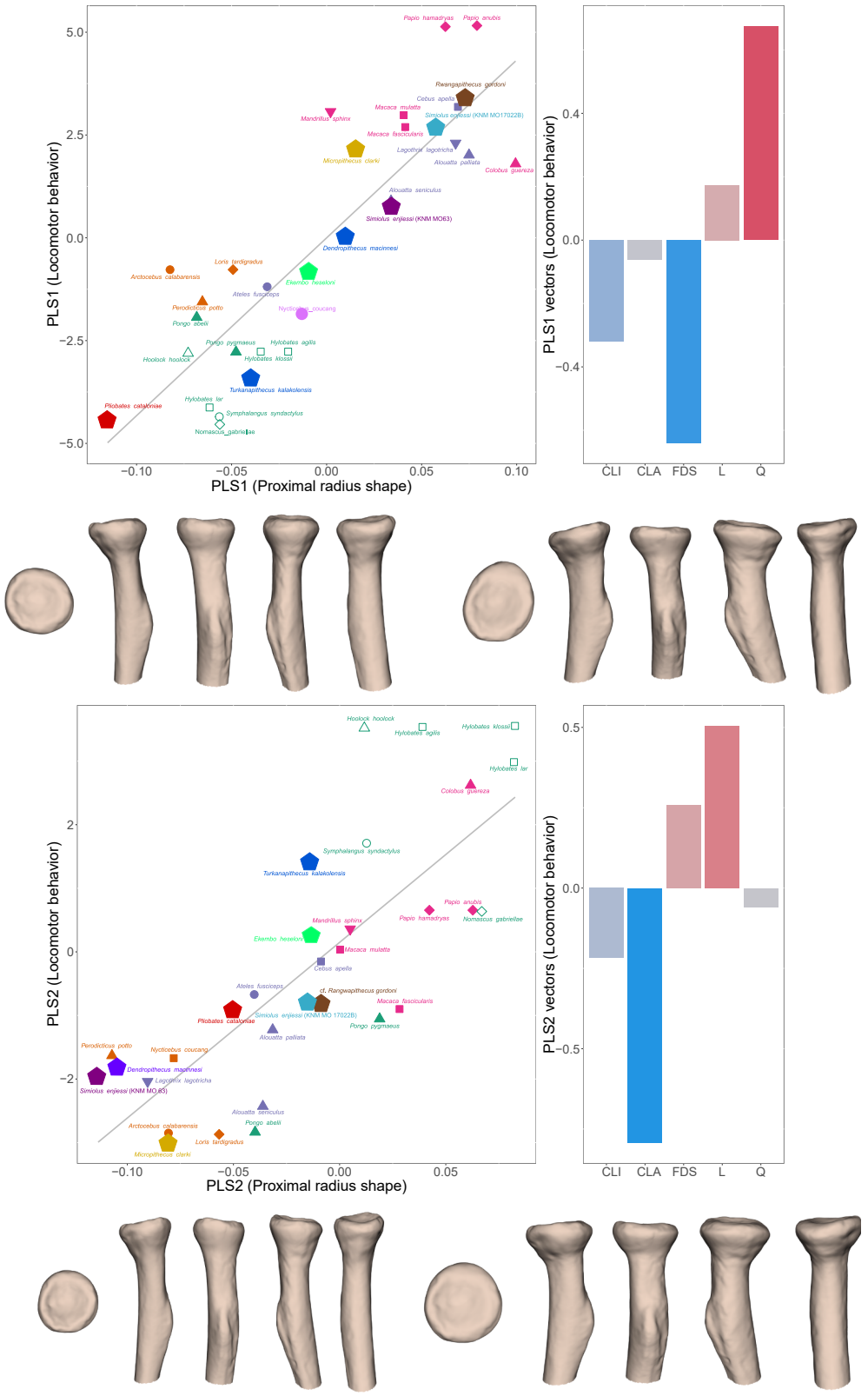


*(legend on next page)*

other end of PLS1 (positive values), quadrupedal taxa cluster together, including cercopithecines, colobines, and the largely quadrupedal platyrrhines, including *Lagothrix*. Shape differences for PLS1 include a round radial head and longer neck at the negative end as opposed to a more oval radial head and a shorter neck at the positive end. Tilting is also recorded at the positive end, being displayed by the non-hominoid primates of the sample. Forelimb-dominated suspension (FDS) and climbing are correlated with negative values in PLS1, whereas quadrupedalism is reflected at the positive end. *Pliobates* falls at the most negative extreme of PLS1, close to hominoids and lorisids. PLS2 (24% of covariance) yields a less clear-cut distribution of extant primate species, with hylobatids and *Colobus guereza* clustering at the positive end and taxa such as *Pongo* and lorisids at the negative end. Shape differences include smaller, slender, and somewhat tilted radial heads in the negative values, as opposed to larger, stouter, and less tilted radial heads in the positive. The positive end of PLS2 is correlated with FDS again, but also with leaping, whereas the negative end is correlated with high frequencies of clambering and, to a lesser extent, climbing. *Pliobates* displays negative values close to the large platyrrhines *Ateles fusciceps* and *Alouatta palliata*.

For the distal radius, there is significant covariation between the shape of the proximal radius and locomotion in the two first PLS axes, accounting for 98% of the total covariance (Figure 5; Table S5). In PLS1 (79% of covariance), hylobatids, *Pongo*, and lorisids are clustered at the positive end, whereas cercopithecoids, quadrupedal large-bodied platyrrhines (e.g., *Alouatta*), and cebids fall at the negative end, with *Ateles* being in intermediate positions. Shape differences depict mediolaterally shorter distal radii at the negative end, with more proportionate lunate-scaphoid facets as well as more prominent radial styloids. The PLS1 is positively correlated with FDS and, to a lesser extent, climbing and negatively with quadrupedalism. *Pliobates* falls close to the cluster at the positive end (including hominoids and lorisids) but displays less positive values overall, being also close to *Ateles*. In PLS2 (18% of covariance), the positive end includes most hylobatids and *Colobus*, whereas lorisids cluster at the negative end, and orangutans, platyrrhines, and cercopithecoids display rather intermediate values (albeit *Pongo abelii* displays more negative values, closer to lorisids). Shape differences include a narrower and smaller ulnar notch and little styloid protrusion at the negative, whereas, at the positive end, the ulnar notch is wider, the styloid of the radius protrudes distally, and the distal radius is narrower mediolaterally. The PLS2 is positively driven by leaping and negatively by clambering and climbing. *Pliobates* displays a somewhat positive value for PLS2 and is found among cercopithecoids but also close to atelids and other fossils.

For the whole radius, the first two PLS show a significant covariation (up to 94% of covariance) between the shape of the whole radius and locomotion (Table S5; Figures S14A and S14B). In PLS1 (78% of covariance), hylobatids cluster at the positive end, followed by *Pongo* and *Ateles*, as well as *Epipliopithecus* and *Pliobates*. Lorisids have intermediate values but, once again, *Perodicticus* shows negative values for radial shape, thus being separated from all other taxa. Cercopithecoids generally show negative values and cluster at the negative and of PLS1. This axis is characterized by lender and straight radii at the positive end and short and robust radii with a markedly curved shaft at the negative. PLS1 is correlated with FDS at its positive end and quadrupedalism at its negative. No clear group distribution is observed in PLS2 (15% of covariance), although it is characterized by more robust radii at the positive end and slenderer at the negative, and it is correlated with clambering and climbing (to a lesser extent) at its positive end, with leaping at its negative.

Based on the proximal radius, the locomotor repertoire inferred for *Pliobates* (Figure 6; Table S6) indicates a high reliance on FDS (50%), coupled with clambering (32%) and climbing (15%). In turn, the distal epiphysis indicates a higher reliance on quadrupedalism (35%), together with FDS (22%) and clambering (16%), and the locomotor repertoire inferred from the whole radius for *Pliobates* includes a moderate reliance in clambering (44%), followed by quadrupedalism (24%) and FDS (22%; Table S6). Percentages of leaping are smaller for all datasets (0%,13%, and 15%, respectively). In locomotor terms, based on the proximal radius, *Pliobates* is thus most similar to the suspensory hylobatids on the one hand and the climbing-clambering *Ateles* and *Alouatta palliata*, on the other. Compared with extinct taxa, *Pliobates* is more similar to *Turkanapithecus* and, to a lesser extent, *Ekembo*, in their respectively inferred percentages of FDS. *Pliobates* is also similar in climbing percentages to these stem hominoids but dissimilar to all extinct taxa in the high amount of clambering inferred, being notably dissimilar overall to the other pliopithecoid in the sample, *Epipliopithecus*, which is predicted to rely on quadrupedalism first and climbing second, with negligible frequencies of other behaviors. For the distal radius, *Pliobates* is most similar to the somewhat suspensory *Ateles* and lorisids on the one hand and *Symphalangus* and other taxa with moderate leaping percentages on the other. Compared with the extinct taxa, *Pliobates* is more similar in FDS percentage to *Turkanapithecus*, while displaying similar frequencies of quadrupedalism to *Limnopithecus*, and being again quite dissimilar overall to *Epipliopithecus*.

## DISCUSSION

### The locomotor repertoire of *Pliobates*

Prior to *Pliobates*, the scarce available postcranials of crouzeliid pliopithecoids[12,34,35] were indicative of (semi)arboreal quadrupedalism with strong climbing abilities and a variable component of suspensory behaviors.[12,34] In turn, the best-known pliopithecid

**Figure 4. Results of the partial least-squares regression (PLSR) analysis for the proximal radius without African apes**

PLS1 is depicted at the top and PLS2 at the bottom. The 3D models of the minimum and maximum radial shape changes for both PLS (PLS1: top; PLS2: bottom) are warped onto a 3D model of a left proximal radius of a hylobatid (*Hylobates agilis* AMNH 106575h) and shown in proximal, posterior, medial, anterior, and lateral views. Data points are color- and symbol-coded: hominoids are in green (hominids in filled symbols, hylobatids in outlines), platyrrhines in purple, cercopithecoids in pink, and lorisids in orange. Fossil specimens are denoted by colored pentagons. CLI, climbing; CLA, clambering; FDS, forelimb-dominated suspension; L, leaping; Q, quadrupedalism.

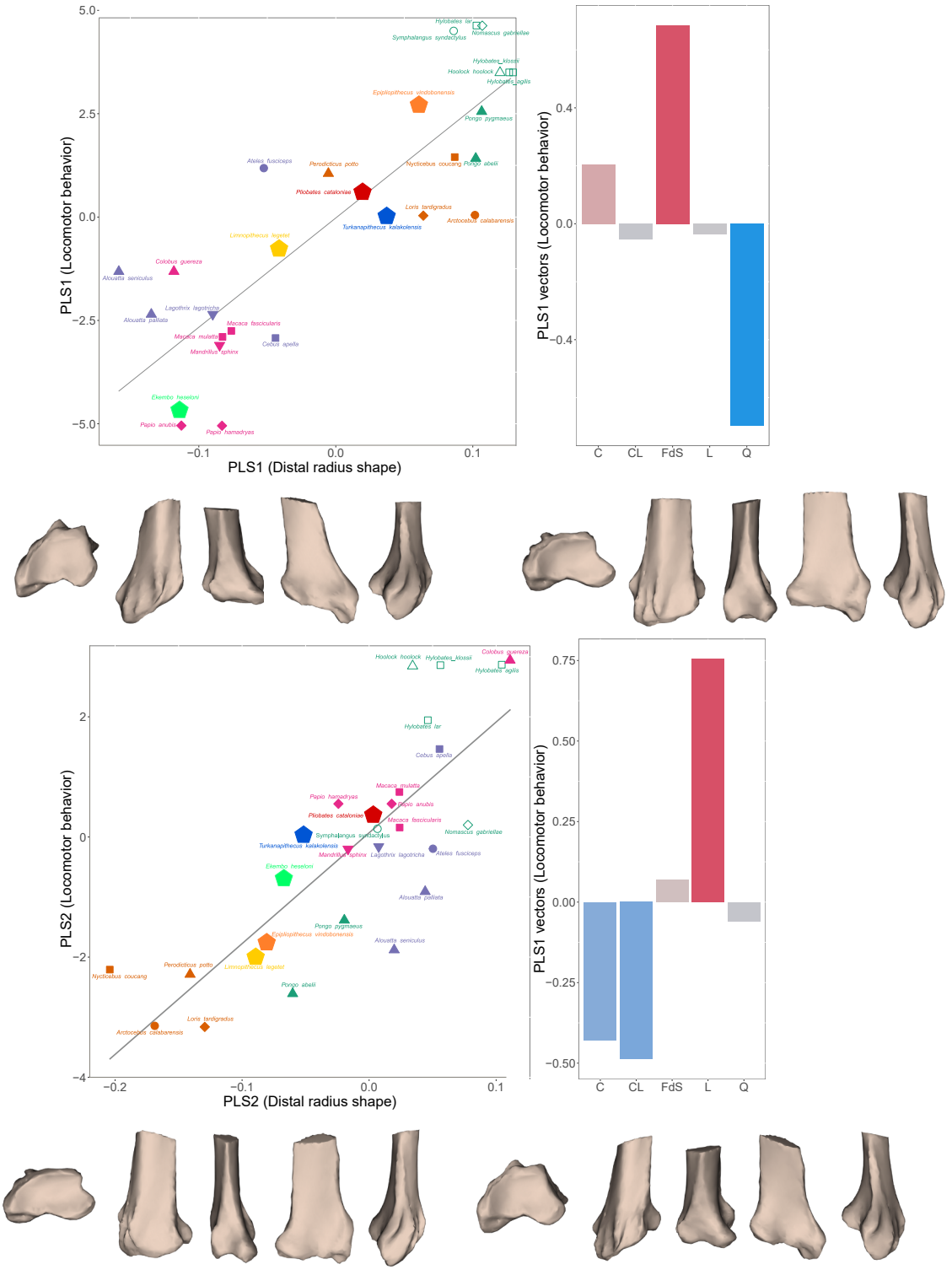


**Figure 5. Results of the partial least-squares regression (PLSR) analysis for the distal radius without African apes**

PLS1 is depicted at the top and PLS2 at the bottom. The 3D models of the minimum and maximum radial shape changes for both PLS (PLS1: top; PLS2: bottom) are warped onto a 3D model of a proximal radius of a chimpanzee (*Pan troglodytes* USNM 220063) and shown in distal, posterior, medial, anterior, and lateral views. Data points are color- and symbol-coded: hominoids are in green (hominids in filled symbols, hylobatids in outlines), platyrrhines in purple, cercopithecoids in pink, and lorisids in orange. Fossil specimens are denoted by colored pentagons. CLI, climbing; CLA, clambering; FDS, forelimb-dominated suspension; L, leaping; Q, quadrupedalism.

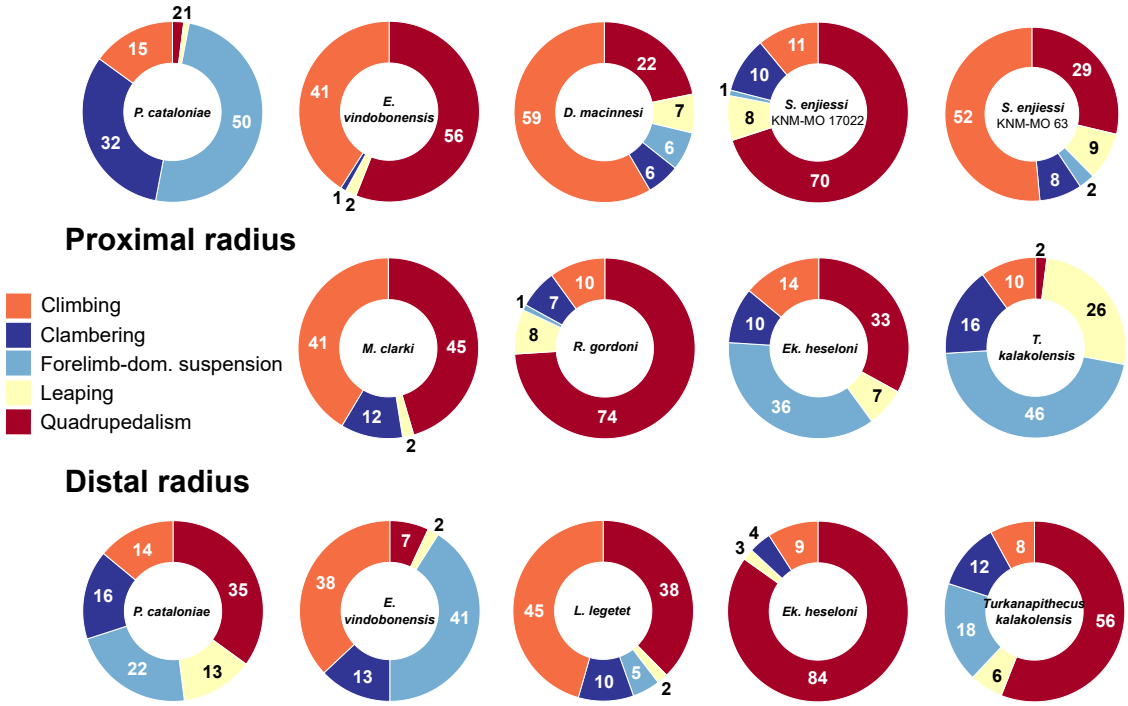


**Figure 6. Locomotor percentage predictions**

Donut plots with the predicted locomotor behaviors for all fossils, including the predictions for the proximal (upper two rows) and distal (lower row) radius. CLI, climbing; CLA, clambering; FDS, forelimb-dominated suspension; L, leaping; Q, quadrupedalism.

(*Epipliopithecus*) is regarded as an arboreal quadruped with some degree of suspensory behaviors.[30,36–38] However, none of these taxa, including those for which the radius is known (*Barberapithecus* and *Epipliopithecus*), show marked similarities with extant apes as is the case of this anatomical area in *Pliobates*. In particular, the morphology of the radial head in *Pliobates*—characterized by a round head, a beveled articular surface extending all around the circumference of the head, minimal tilt, and absence of a lateral lip—closely resembles that of extant hominoids.[1,5,9,11,39–42] This ape-like configuration includes the medial orientation of the radial tuberosity—not lateral as incorrectly reported in the original description.[5] The tuberosity is variably located in primates, mostly ranging from anterior to medial.[40] However, hominoids generally exhibit a medially facing tuberosity (Figure S9). As previously noted,[5] the ape-like characteristics of the proximal radius of *Pliobates* facilitate a wide range of prono-supination, essential for a highly mobile radiohumeral joint.[5,11,12,40–42] In extant hominoids, such radial head morphology enhances joint stabilization during suspensory and climbing behaviors, where the articulation of the radial head with the zona conoidea of the humerus and the radial notch of the ulna allows for consistent contact throughout the prono-supination range.[9,41] Despite this ape-like humeroradial configuration, *Pliobates* lacks the full set of traits functionally related to suspensory locomotion typical of extant apes. *Pliobates* combines an ape-like morphology of the radiohumeral joint with a plesiomorphic humeroulnar joint, lacking morphological traits that are critical to stabilization, such as the median keel of the ulna.[13] Likewise, such functional decoupling can be observed in the distal humerus of *Pliobates*,[5,43] where the humeral capitulum (i.e., the proximal radius counterpart) is globular and indicates a wide range of movement, whereas the humeral trochlea is not waisted and does not display a developed lateral keel. This humeroulnar morphology, in the extant apes, is key for stabilizing the elbow against the mediolateral loadings during forelimb-dominated (i.e., with full weight-bearing and no use of other supports) suspension (ranging from arm-swinging, which is slower, to ricochetal brachiation, which is the most extreme form of FDS). Moreover, this ape-like humeroradial morphology is not only displayed by taxa engaging in FDS but also by other taxa, such as lorisids (as seen in our morphological analyses), which are suspensory primates but do not engage in FDS. They suspend mostly from the hindlimbs, and, when engaging in forelimb traction behaviors (i.e., those putting the forelimbs in tension), they typically also engage the hindlimbs (e.g., during clambering, [vertical] climbing, or inverted quadrupedalism). As such, it appears that an ape-like radial morphology is functionally related to enhanced prono-supination at the humeroradial joint (i.e., forearm rotation), which is useful for both suspensory and climbing/clambering behaviors. The *Pliobates* elbow—characterized by a plesiomorphic humeroulnar joint and a humeroradial joint providing for extensive, efficient, and stable forearm rotation—appears adapted for cautious, eclectic climbing rather than for primarily engaging in forelimb-dominated acrobatic suspension.

While the proximal radius of *Pliobates* is modern-ape-like, its distal radius retains more plesiomorphic features compared with that of hominoids, alongside with the presence of some ape-like traits. Notably, the ulnar notch is wide to accommodate

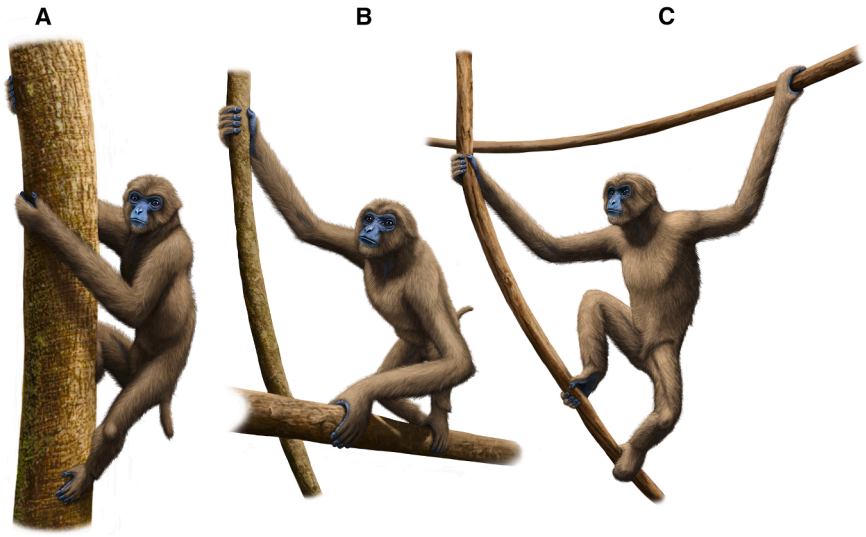


**Figure 7. The locomotor behaviors of *Pliobates cataloniae***

Based on previous papers and our results based on the radius, *Pliobates* would have been able to perform a diverse array of locomotor behaviors, including the following:
(A) Vertical climbing.
(B) Clambering.
(C) Quadrumanous suspension.

an expanded ulnar head resembling that of hominoids.[5,13] This morphology is paired with a somewhat enlarged lunate facet at the distal radius, although not to the extent observed in hominoids and lorisids, where the lunate facet is much larger than the scaphoid facet.[44] Plesiomorphic traits include a more prominent radial styloid in *Pliobates* than in hominoids, resembling that of cercopithecoids and platyrrhines.[44] Thus, the distal radius of *Pliobates* displays a mosaic morphology, unique in its radiocarpal articulation, lacking an extant analog. The expanded ulnar notch aligns with enhanced prono-supination capabilities at the wrist, facilitated by a diarthrodial articulation at the distal radioulnar joint, as in hominoids and lorisids,[9,13,32] while the size and shape of the carpal facets suggest versatility in wrist postures,[38] although not as diverse as in extant hominoids or early hominins. Such configuration is most suited to support weight in semipronated and fully pronated positions while still allowing for wide rotational capabilities at the distal forearm and enhanced wrist mobility. These capabilities combined are suitable for branch-grasping during climbing or palmigrade quadrupedalism—as further indicated by the results of our locomotor frequency analyses—and clearly deviate from the condition of palmigrade and digitigrade extant anthropoids, in which the mobility of the wrist is limited, for example, by a full articulation between the styloid of the ulna and the carpus, as well as a reduced radioulnar articulation that limits the rotational range of the radius.[9,13,32]

This notwithstanding, FDS behaviors probably constituted a non-negligible portion of the locomotor repertoire of *Pliobates*. This is supported by the long and slender radius, which displays an estimated degree of forelimb elongation similar to that of female orangutans and woolly spider monkeys[5] and further possesses a long and straight shaft, as well as an elongated radial neck, similarly to hylobatids. The radius is particularly long relative to humeral length (albeit less so than in hylobatids and *Ateles*[5]), which together with the ape-like traits of the proximal and distal radius, the high arm angle (i.e., the carrying angle of the elbow or the angle between the long axes of the humerus and ulna[9]), and the medially facing radial tuberosity[5] are indicative of some degree of below-branch FDS in *Pliobates*. Nevertheless, a predominantly FDS repertoire—as suggested only by the locomotor frequency analysis of the proximal radius—remains unlikely because, as previously argued,[5] the humeroulnar and radiocarpal joints would not have been able to withstand more than moderate or occasional FDS behaviors. With an estimated body mass of ~5 kg, the *Pliobates* elbow might have required less developed mechanisms of passive stabilization during FDS than the considerably larger extant great apes. However, *Pliobates* is about the same size of extant gibbons (*Hylobates*, *Hoolock*, and *Nomascus*), and yet it lacks the striking adaptations of the latter (e.g., a true ball-and-socket joint at the wrist, enabling 180° of rotation)[45] for a higher reliance on suspensory behaviors, including ricochetal brachiation.[46] *Ateles* (spider monkeys), with a slightly larger body mass (~5–9 kg), similarly lack key stabilizing elements for suspensory behaviors at the humeroulnar joint (such as the median keel in the trochlear notch of the ulna[11,13]) despite being convergent in radial head morphology with extant hominoids. *Ateles* engages in tail-assisted brachiation (without a flight phase) for up to ~50% of its locomotor repertoire, depending on the species,[47] but its prehensile tail mitigates some of the mechanical stresses imposed on the forelimbs during suspensory locomotion.[48] While the tail morphology of *Pliobates* is unknown, tail-assisted brachiation may be reasonably discounted, as a prehensile tail is only present in extant atelids and has never been suggested for any extinct catarrhine.[49] Considering all the available evidence for the *Pliobates* elbow, its locomotor repertoire would have likely involved the use of non-stereotypical postures of the forelimb, perhaps including quadrumanous suspension (i.e., using both the fore- and the hindlimbs) to a larger extent than FDS, in addition to other arboreal behaviors such as quadrupedalism, climbing, and clambering (as supported by our results)—overall indicating a highly eclectic, diverse, and versatile locomotor repertoire (Figure 7).

## Locomotor evolution in catarrhines

When considering the radius alongside the ulna[13] and the distal humerus,[5,43] the forelimb of *Pliobates* appears well adapted to a broad range of prono-supination, which would have enabled the forearm to reach in various directions during non-stereotypical postures required for many arboreal locomotor behaviors, including climbing alongside quadrupedalism, while being overall highly varied. Together with other fossils in our sample, our refined inferences of the locomotor repertoire of *Pliobates* have broader

implications for the evolution of forelimb morphology and locomotion in catarrhines. Dendropithecids (*Simiolus*, *Dendropithecus*, and *Micropithecus*) more closely resemble the proximal radial condition of the crown catarrhine ancestral morphotype[12] than any of the other fossils analyzed here. Unlike *Pliobates*, but like other pliopithecoids (*Epipliopithecus* and *Barberapithecus*), dendropithecids are much more plesiomorphic in radial morphology than crown catarrhines (particularly hominoids), displaying features—such as a lateral lip, oval outline of the radial head, prominent styloid, and relatively short length—that support elbow stability in flexed and pronated elbow postures corresponding to the weight-bearing phase of the quadrupedal gait.[11,40]

The proximal and distal radius of Early and Middle Miocene apes, such as *Ekembo*, *Turkanapithecus*, *Equatorius*, and *Nacholapithecus*,[12,42] show an intermediate morphology between the crown catarrhine and the crown hominoid ancestral morphotypes, likely reflecting a trade-off between joint mobility (functionally related to the use of the elbow in varying postures) and elbow stability during quadrupedal behaviors. An exception is the proximal radius of the early nyanzapithecid *Rangwapithecus*[39] (~20 Ma), alternatively attributed to *Proconsul africanus*,[35] which resembles that of dendropithecids and *Epipliopithecus*. The radius of *Rangwapithecus* is clearly plesiomorphic compared with *Ekembo* and other Miocene apes, including the slightly younger (~17 Ma) nyanzapithecid *Turkanapithecus*, which exhibits proximal and distal radial epiphysis more similar to those of crown hominoids.[11] This is also the case of the Middle Miocene (~15 Ma) *Nacholapithecus*, at least, for the proximal epiphysis,[42] whereas the distal is overall more similar to that of *Ekembo*.[50] Both taxa illustrate early acquisitions (~17–15 Ma) of modern-ape-like features, despite lacking any adaptations for suspensory locomotion.[11,51] This contradicts the view that FDS was the main adaptive driver of forelimb morphology (e.g., the radiohumeral joint) in ape evolution, to the exclusion of other locomotor behaviors.

The elbow joint morphology of crown hominoids has been customarily interpreted in the framework of their characteristic orthograde (upright torso) body plan[52–54]—considered by some authors to be a synapomorphic morphofunctional complex that originated as a suspensory adaptation.[15–17,19–21,54,55] However, such assumption has been challenged in the light of elbow and other postcranial similarities between hominoids and other primates such as lorisids and atelids,[14,32,33] as well as the more plesiomorphic postcranial morphology and lack of specific suspensory adaptations in Miocene great apes such as *Sivapithecus*[56] and *Pierolapithecus*.[23,24] Until current uncertainties about the phylogenetic relationships between Miocene and extant apes are clarified (see review in Urciuoli and Alba[28]), it will be difficult to discern to what extent the derived elbow traits shared by hylobatids and hominids are synapomorphic or homoplastic. Nevertheless, the radius of *Pliobates*, which belongs to a different catarrhine clade, not only reinforces the prevalence of homoplasy in catarrhine forelimb evolution but clearly supports the view that the modern-ape-like elbow complex must not necessarily represent an integrated morphofunctional adaptive complex. Rather the contrary, the radius of *Pliobates* supports that such features evolved in a stepwise fashion and that some of them (particularly, those of the proximal radius) might not have been originally selected for suspension but for other arboreal behaviors that also benefit from extensive forearm prono-supination and stabilization across a broad range of elbow motion (such as climbing and clambering)—even if later co-opted by crown hominoids for FDS.[1,23,24,27,28]

This view is supported not only by the early acquisition of modern-ape-like radiohumeral (and, to a lesser extent, distal radioulnar) features in the hominoid lineage (~17 Ma) but also, and especially, by the distal radial morphology of *Pliobates*. The latter is overall much more plesiomorphic than the proximal radial morphology of the same taxon (and even more so than that of other extinct catarrhines, such as *Epipliopithecus* and *Turkanapithecus*), revealing a trade-off of the locomotor-related selective pressures acting on the radius as a whole. Even though each linage has its own evolutionary history, *Pliobates* offers a compelling example of the evolutionary decoupling between the humeroradial and the humeroulnar joints—with the former displaying an apelike condition (functionally suitable for climbing and/or suspension) and the latter displaying a much more plesiomorphic condition (lacking features specifically related to FDS).[23,27] As such, the radial morphology of *Pliobates* resembles the condition of some Miocene apes, which likely represents an evolutionary stage preceding the acquisition of FDS adaptations. Overall, these findings highlight the mosaic nature of catarrhine elbow evolution and reinforce the view that key features of the crown hominoid elbow complex likely evolved under changing selective pressures related to the progressive acquisition of new locomotor behaviors through time.

## Limitations of the study

The locomotor data have been compiled from the literature and do not represent the complete spectrum of locomotor behaviors exhibited by the extant primates included in the analyses. While this is preferable for making locomotor inferences to using a single locomotor category for each primate taxon (given their diverse locomotor repertoires), it also poses some limitations for the study. Methodologically, for some of the taxa, data are not complete (i.e., their full locomotor repertoire is not known, or only some aspects such as arboreal behaviors have been studied), whereas for some others locomotor data do not even exist and have been extrapolated from their closest available counterparts. Nevertheless, this approach is intended for elucidating which behaviors are most related or have the most predictive power with respect to the morphology under study, such that the inferred locomotor percentages should not be taken literally.

Moreover, deriving locomotor inferences from a single bone is a clear limitation of any study of this kind, as each bone (or even different epiphyses from a single bone) is subject to different selective pressures depending on the role of each anatomical area in the considered locomotor behaviors. Efforts have been made to present our findings considering the larger picture (the total morphological pattern[57]) of what is currently known about the postcranial morphology of *Pliobates* and catarrhines more broadly. To infer the locomotor repertoire of any given extinct taxon for which more than a single skeletal structure is known, as in the case of *Pliobates*, the trade-offs evidenced by the divergent estimates provided by each anatomical structure should be considered within a proper morphofunctional framework. Incomplete and fragmentary preservation constitutes the main

challenge for making paleobiological inferences of locomotion in extinct taxa. *Pliobates*, however, is represented by a partial skeleton that further preserves hindlimb and hand elements that should be considered in future studies and will allow to test further the conclusions derived in this paper—particularly, in relation to the potential role of hindlimb suspension and other behaviors that might be better reflected by the hand or the hindlimb, such as vertical climbing.

More broadly, given the mosaic nature of evolution and the pervasiveness of homoplasy, current uncertainties and ongoing debate surrounding the phylogenetic relationships of Miocene apes and other extinct catarrhines (particularly, relative to their extant counterparts) hinder reaching sounder conclusions about the emergence of locomotor adaptations during the evolutionary history of this group.[28] New fossil findings of stem hylobatids and African great apes are necessary to better reconstruct the ancestral morphotypes from which extant lineages arose.

## RESOURCE AVAILABILITY

### Lead contact

Requests for further information and resources should be directed to and will be fulfilled by the lead contact, Julia Arias-Martorell (julia.arias@icp.cat).

### Materials availability

This study did not generate new unique reagents.

### Data and code availability

- Raw landmark data have been deposited in Mendeley (DOI: https://doi.org/10.17632/dk7nhc9jjy.1) and are publicly available as of the date of publication.
- The 3D model of the radius of *Pliobates cataloniae* has been deposited in MorphoSource and is publicly available (after request and approval) at ark:/87602/m4/769006 as of the date of publication. A dataset with the extant sample used in this study with the corresponding DOI or ARK from MorphoSource for quick access has also been deposited in Mendeley (DOI: https://doi.org/10.17632/pp4bcpvv5n.1); most specimens are publicly available without restriction except some individuals (in which case this is clearly marked in the dataset) that are available upon request as of the date of publication.
- This paper does not report original code.
- Any additional information required to reanalyze the data reported in this paper is available from the lead contact upon request.

## ACKNOWLEDGMENTS

This publication is part of the R+D+I projects PID2020-116908GB-100/AEI/10.13039/501100011033/ (to J.A.-M. and S.M.-S.) and PID2020-117289GB-100/AEI/10.13039/501100011033/(to D.M.A.) funded by the Agencia Estatal de Investigación (AEI) of the Ministerio de Ciencia e Innovación from Spain, and part of the project PID2024-159434NB-I00/AEI/10.13039/501100011033/ (to J.A.-M. and D.M.A.), funded by the AEI of the Ministerio de Ciencia, Innovación y Universidades and ERDF, EU Research has also been funded by the Generalitat de Catalunya/CERCA Program (to J.A.-M., G.R.-I., O.M.-G., A.U., J.G., S.M.-S., and D.M.A.); the Agència de Gestió d'Ajuts Universitaris i de Recerca of the Generalitat de Catalunya (consolidated research groups 2022 SGR 00620 to D.M.A. and J.G. and 2022 SGR 01188 to S.M.-S., J.A.-M., G.R.-I., and A.U.); the Departament de Cultura of the Generalitat de Catalunya (CTL_0009_22_000018 to D.M.A.); a predoctoral grant from the Ministerio de Ciencia e Innovación (PRE2021-09911 to G.R.-I.); a Joan Oró predoctoral grant from the Agència de Gestió d'Ajuts Universitaris i de Recerca of the Generalitat de Catalunya (2023 FI-3 00131 to O.M.-G.); and the grant JSPS Kakenhi 23K27253 (to M.N.). The authors thank S. Almécija for providing 3D models of extant and fossil specimens, as well as landmark descriptions, and for helpful comments about an earlier version of this manuscript. We would also like to thank two anonymous reviewers and the Academic Editor for their useful comments, which helped us improve an earlier version of this article.

## AUTHOR CONTRIBUTIONS

Conceptualization, J.A.-M. and D.M.A.; methodology, J.A.-M., G.R.-I., O.M.-G., and A.U.; investigation, J.A.-M., D.M.A., and S.M.-S.; writing—original draft, J.A.-M. and D.M.A.; writing—review & editing, G.R.-I., O.M.-G., J.G., S.M.-S., and M.N.; funding acquisition, S.M.-S., D.M.A., and J.A.-M.; resources, M.N., S.M.-S., and D.M.A.; supervision, D.M.A; artwork, J.G.

## DECLARATION OF INTERESTS

The authors declare no competing interests.

## STAR★METHODS

Detailed methods are provided in the online version of this paper and include the following:

- KEY RESOURCES TABLE
- EXPERIMENTAL MODEL AND STUDY PARTICIPANT DETAILS
  - Fossil sample
  - Extant sample
- METHOD DETAILS
  - Scanning methods
  - Fossil dates
- QUANTIFICATION AND STATISTICAL ANALYSIS
  - Landmark protocols
  - 3D geometric morphometric analyses
  - Locomotor frequency analysis
- ADDITIONAL RESOURCES
  - Morphosource

## SUPPLEMENTAL INFORMATION

Supplemental information can be found online at https://doi.org/10.1016/j.isci.2025.114622.

Received: September 19, 2025
Revised: November 13, 2025
Accepted: December 30, 2025
Published: January 3, 2026

## REFERENCES

1. Bouchet, F., Zanolli, C., Urciuoli, A., Almécija, S., Fortuny, J., Robles, J.M., Beaudet, A., Moyà-Solà, S., and Alba, D.M. (2024). The Miocene primate *Pliobates* is a pliopithecoid. Nat. Commun. *15*, 2822. https://doi.org/10.1038/s41467-024-47034-9.
2. Bouchet, F., Zanolli, C., Skinner, M.M., Urciuoli, A., Fortuny, J., Almécija, S., Bernardini, F., Tuniz, C., Schillinger, B., Moyà-Solà, S., and Alba, D.M. (2024). Molar enamel–dentine junction shape of *Pliobates cataloniae* and other Iberian pliopithecoids. J. Hum. Evol. *195*, 103581. https://doi.org/10.1016/j.jhevol.2024.103581.
3. Begun, D.R. (2002). The Pliopithecoidea. In The Primate Fossil Record, W.C. Hartwig, ed. (Cambridge University Press), pp. 221–240.
4. Harrison, T. (2013). Catarrhine origins. In A Companion to Paleoanthropology, D.R. Begun, ed. (Blackwell Publishing), pp. 376–396.
5. Alba, D.M., Almécija, S., DeMiguel, D., Fortuny, J., Pérez de los Ríos, M., Pina, M., Robles, J.M., and Moyà-Solà, S. (2015). Miocene small-bodied ape from Eurasia sheds light on hominoid evolution. Science *350*, aab2625. https://doi.org/10.1126/science.aab2625.

6. Nengo, I., Tafforeau, P., Gilbert, C.C., Fleagle, J.G., Miller, E.R., Feibel, C., Fox, D.L., Feinberg, J., Pugh, K.D., Berruyer, C., et al. (2017). New infant cranium from the African Miocene sheds light on ape evolution. Nature *548*, 169–174. https://doi.org/10.1038/nature23456.

7. Gilbert, C.C., Ortiz, A., Pugh, K.D., Campisano, C.J., Patel, B.A., Singh, N.P., Fleagle, J.G., and Patnaik, R. (2020). New middle Miocene ape (Primates: Hylobatidae) from Ramnagar, India fills major gaps in the hominoid fossil record. Proc. Biol. Sci. *287*, 20201655. https://doi.org/10.1098/rspb.2020.1655.

8. Ji, X., Harrison, T., Zhang, Y., Wu, Y., Zhang, C., Hu, J., Wu, D., Hou, Y., Li, S., Wang, G., and Wang, Z. (2022). The earliest hylobatid from the Late Miocene of China. J. Hum. Evol. *171*, 103251. https://doi.org/10.1016/j.jhevol.2022.103251.

9. Sarmiento, E.E. (1985). Functional Differences in the Skeleton of Wild and Captive Orangutans and their Adaptive Significance Ph.D. thesis (New York University), p. 594.

10. Sarmiento, E.E., Stiner, E., and Mowbray, K. (2002). Morphology-based systematics (MBS) and problems with fossil hominoid and hominid systematics. Anat. Rec. *269*, 50–66. https://doi.org/10.1002/ar10055.

11. Rose, M.D. (1993). Functional anatomy of the elbow and forearm in primates, Postcranial Adaptations in Nonhuman Primates. and D.L. Gebo, eds. (Northern Illinois Univ. Press), pp. 70–95.

12. Arias-Martorell, J., Almécija, S., Urciuoli, A., Nakatsukasa, M., Moyà-Solà, S., and Alba, D.M. (2021). A proximal radius of *Barberapithecus huerzeleri* from Castell de Barberà: Implications for locomotor diversity among pliopithecoids. J. Hum. Evol. *157*, 103032. https://doi.org/10.1016/j.jhevol.2021.103032.

13. Raventós-Izard, G., Monclús-Gonzalo, O., Moyà-Solà, S., Alba, D.M., and Arias-Martorell, J. (2025). Ulnar morphology of *Pliobates cataloniae* (Pliopithecoidea: Crouzeliidae): Insights into catarrhine locomotor diversity and forelimb evolution. J. Hum. Evol. *202*, 103663. https://doi.org/10.1016/j.jhevol.2025.103663.

14. Larson, S.G. (1998). Parallel evolution in the hominoid trunk and forelimb. Evol. Anthropol. *6*, 87–99. https://doi.org/10.1002/(SICI)1520-6505(1998)6:3<87::AID-EVAN3>3.0.CO;2-T.

15. Keith, A. (1902). The extent to which the posterior segments of the body have been transmuted and suppressed in the evolution of man and allied primates. J. Anat. Physiol. *37*, 18–40.

16. Keith, A. (1923). Hunterian lectures on man's posture: Its evolution and disorders. Lecture I. Theories concerning the evolution of man's posture. Br. Med. J. *1*, 451–454.

17. Keith, A. (1923). Hunterian lectures on man's posture: Its evolution and disorders. Lecture II. The evolution of the orthograde spine. Br. Med. J. *1*, 499–502. https://doi.org/10.1136/bmj.1.3246.451.

18. Benton, R.S. (1974). Structural patterns in the Pongidae and Cercopithecidae. Yearb. Phys. Anthropol. *18*, 65–88.

19. Tuttle, R.H. (1975). Parallelism, brachiation, and hominoid phylogeny. In Phylogeny of the Primates: A Multidisciplinary Approach, T.J. Luckett and F. Szalay, eds. (Plenum Press), pp. 447–480.

20. Pilbeam, D. (1996). Genetic and morphological records of the Hominoidea and hominid origins: a synthesis. Mol. Phylogenet. Evol. *5*, 155–168. https://doi.org/10.1006/mpev.1996.0010.

21. Harrison, T., and Rook, L. (1997). Enigmatic anthropoid or misunderstood ape? The phylogenetic status of *Oreopithecus bambolii* reconsidered. In Function, Phylogeny, and Fossils: Miocene Hominoid Evolution and Adaptations, D.R. Begun, C.V. Ward, and M.D. Rose, eds. (Plenum Press), pp. 327–362.

22. Williams, S.A., Prang, T.C., Russo, G.A., Young, N.M., and Gebo, D.L. (2023). African apes and the evolutionary history of orthogrady and bipedalism. Am. J. Biol. Anthropol. *181*, 58–80. https://doi.org/10.1002/ajpa.24684.

23. Moyà-Solà, S., Köhler, M., Alba, D.M., Casanovas-Vilar, I., and Galindo, J. (2004). *Pierolapithecus catalaunicus*, a new Middle Miocene great ape from Spain. Science *306*, 1339–1344. https://doi.org/10.1126/science.1103094.

24. Alba, D.M. (2012). Fossil apes from the Vallès-Penedès Basin. Evol. Anthropol. *21*, 254–269. https://doi.org/10.1002/evan.21312.

25. Pilbeam, D., Rose, M.D., Barry, J.C., and Shah, S.M. (1990). New *Sivapithecus* humeri from Pakistan and the relationship of *Sivapithecus* and *Pongo*. Nature *348*, 237–239. https://doi.org/10.1038/348237a0.

26. Madar, S.I., Rose, M.D., Kelley, J., MacLatchy, L., and Pilbeam, D. (2002). New *Sivapithecus* postcranial specimens from the Siwaliks of Pakistan. J. Hum. Evol. *42*, 705–752. https://doi.org/10.1006/jhev.2002.0554.

27. Almécija, S., Hammond, A.S., Thompson, N.E., Pugh, K.D., Moyà-Solà, S., and Alba, D.M. (2021). Fossil apes and human evolution. Science *372*, eabb4363. https://doi.org/10.1126/science.abb4363.

28. Urciuoli, A., and Alba, D.M. (2023). Systematics of Miocene apes: State of the art of a neverending controversy. J. Hum. Evol. *175*, 103309. https://doi.org/10.1016/j.jhevol.2022.103309.

29. Alba, D.M., Urciuoli, A., Hammond, A.S., Almécija, S., Rook, L., and Zanolli, C. (2024). Miocene ape evolution: Where does *Oreopithecus* fit in? Boll. Soc. Paleontol. Ital. *63*, 153–182. https://doi.org/10.4435/BSPI.2024.01.

30. Arias-Martorell, J., Tallman, M., Potau, J.M., Bello-Hellegouarch, G., and Pérez-Pérez, A. (2015). Shape analysis of the proximal humerus in orthograde and semi-orthograde primates: correlates of suspensory behavior. Am. J. Primatol. *77*, 1–19. https://doi.org/10.1002/ajp.22306.

31. Pugh, K.D. (2022). Phylogenetic analysis of Middle–Late Miocene apes. J. Hum. Evol. *165*, 103140. https://doi.org/10.1016/j.jhevol.2021.103140.

32. Cartmill, M., and Milton, K. (1977). The lorisiform wrist joint and the evolution of "brachiating" adaptations in the Hominoidea. Am. J. Phys. Anthropol. *47*, 249–272. https://doi.org/10.1002/ajpa.1330470206.

33. Sarmiento, E.E. (1995). Cautious climbing and folivory: a model of hominoid differentiation. Hum. Evol. *10*, 289–321. https://doi.org/10.1007/BF02438967.

34. Begun, D.R. (1993). New catarrhine phalanges from Rudabánya (Northeastern Hungary) and the problem of parallelism and convergence in hominoid postcranial morphology. J. Hum. Evol. *24*, 373–402. https://doi.org/10.1006/jhev.1993.1028.

35. Senut, B. (2012). Les restes post-crâniens des Pliopithecidae (Primates) de Sansan. Mem. Mus. Natl. Hist. Nat. *203*, 535–558.

36. Zapfe, H. (1961). Ein Primatenfund aus der miozänen Molasse von Oberösterreich. Z. Morphol. Anthropol. *52*, 247–267.

37. Bacon, A.M. (1994). Nouvelles perspectives sur la locomotion de *Pliopithecus vindobonensis* (Zapfe et Hürzeler, 1957). C. R. Acad. Sci. Paris *318*, 259–266.

38. Rein, T.R., Harrison, T., and Zollikofer, C.P.E. (2011). Skeletal correlates of quadrupedalism and climbing in the anthropoid forelimb: implications for inferring locomotion in Miocene catarrhines. J. Hum. Evol. *61*, 564–574. https://doi.org/10.1016/j.jhevol.2011.07.005.

39. Harrison, T. (1982). Small-bodied Apes from the Miocene of East Africa (Ph.D. Thesis (University College London)).

40. Rose, M.D. (1988). Another look at the anthropoid elbow. J. Hum. Evol. *17*, 193–224. https://doi.org/10.1016/0047-2484(88)90054-1.

41. Rose, M.D. (1983). Miocene hominoid postcranial morphology: monkey-like, ape-like, neither, or both? In New Interpretations of Ape and Human Ancestry, R.L. Ciochon and R.S. Corruccini, eds. (Plenum Press), pp. 405–417.

42. Arias-Martorell, J., Urciuoli, A., Almécija, S., Alba, D.M., and Nakatsukasa, M. (2023). The radial head of the Middle Miocene ape *Nacholapithecus kerioi*: Morphometric affinities, locomotor inferences, and implications for the evolution of the hominoid humeroradial joint. J. Hum. Evol. *178*, 103345. https://doi.org/10.1016/j.jhevol.2023.103345.

43. Figueroa-Torrejón, A., Almécija, S., Moyà-Solà, S., Alba, D.M., and Arias-Martorell, J. (2023). Geometric morphometric analysis of the distal humerus of *Pliobates cataloniae*: Locomotor inferences and anthropoid elbow

evolution. Palaeovertebrata Spec. Vol. *1*, 86–87. https://doi.org/10.18563/pv.eavp2023.

44. Tallman, M. (2012). Morphology of the distal radius in extant hominoids and fossil hominins: Implications for the evolution of bipedalism. Anat. Rec. *295*, 454–464. https://doi.org/10.1002/ar.22405.

45. Preuschoft, H., and Demes, B. (1984). Biomechanics of brachiation. In The Lesser Apes: Evolutionary and Behavioural Biology, H. Preuschoft, D. Chivers, W. Brockelmann, and N. Creel, eds. (Edinburgh Univ. Press), pp. 96–118.

46. Fleagle, J.G. (1976). Locomotion and posture of the Malayan siamang and implications for hominoid evolution. Folia Primatol. *26*, 245–269. https://doi.org/10.1159/000155756.

47. Cant, J.G., Youlatos, D., and Rose, M.D. (2001). Locomotor behavior of *Lagothrix lagothricha* and *Ateles belzebuth* in Yasuní National Park, Ecuador: general patterns and nonsuspensory modes. J. Hum. Evol. *41*, 141–166. https://doi.org/10.1006/jhev.2001.0485.

48. Rose, M.D., Turnquist, J.E., and Lemelin, P. (2005). Role of the prehensile tail during ateline locomotion: experimental and osteological evidence. Am. J. Phys. Anthropol. *126*, 435–446. https://doi.org/10.1002/ajpa.20075.

49. Rose, M.D. (1996). Functional morphological similarities in the locomotor skeleton of Miocene catarrhines and platyrrhine monkeys. Folia Primatol. *66*, 7–14. https://doi.org/10.1159/000157180.

50. Takano, T., Nakatsukasa, M., Kunimatsu, Y., Nakano, Y., Ogihara, N., and Ishida, H. (2018). Forelimb long bones of *Nacholapithecus* (KNM-BG 35250) from the middle Miocene in Nachola, northern Kenya. Anthropol. Sci. *126*, 135–149. https://doi.org/10.1537/ase.181022.

51. Nakatsukasa, M., and Kunimatsu, Y. (2009). *Nacholapithecus* and its importance for understanding hominoid evolution. Evol. Anthropol. *18*, 103–119. https://doi.org/10.1002/evan.20208.

52. Maclatchy, L. (2004). The oldest ape. Evol. Anthropol. *13*, 90–103. https://doi.org/10.1002/evan.10133.

53. MacLatchy, L.M., Cote, S.M., Deino, A.L., Kityo, R.M., Mugume, A.A.T., Rossie, J.B., Sanders, W.J., Cosman, M.N., Driese, S.G., Fox, D.L., et al. (2023). The evolution of hominoid locomotor versatility: Evidence from Moroto, a 21 Ma site in Uganda. Science *380*, eabq2835. https://doi.org/10.1126/science.abq2835.

54. Pilbeam, D.R., and Lieberman, D.E. (2017). Reconstructing the Last Common Ancestor of chimpanzees and humans. In Chimpanzees and Human Evolution, M.N. Muller, R. Wrangham, and D.R. Pilbeam, eds. (Harvard University Press), pp. 22–141. https://www.jstor.org/stable/j.ctv24w65tq.4.

55. Harrison, T. (1991). The implications of *Oreopithecus bambolii* for the origins of bipedalism. In Origine(s) de la Bipédie chez les Hominidés, B. Senut and Y. Coppens, eds. (Editions du CRNS), pp. 235–244.

56. Morgan, M.E., Lewton, K.L., Kelley, J., Otárola-Castillo, E., Barry, J.C., Flynn, L.J., and Pilbeam, D. (2015). A partial hominoid innominate from the Miocene of Pakistan: Description and preliminary analyses. Proc. Natl. Acad. Sci. USA *112*, 82–87. https://doi.org/10.1073/pnas.1420275111.

57. Stern, J.T.J., and Susman, R.L. (1991). "Total morphological pattern" versus the "magic trait": Conflicting approaches to the study of early hominid bipedalism. In Origine(s) de la bipédie chez les hominidés, B. Senut and Y. Coppens, eds. (Editions du CNRS), pp. 99–111.

58. R Core Team. (2021). R: A Language and Environment for Statistical Computing (R Foundation for Statistical Computing). https://www.r-project.org/

59. Schlager, S. (2017). Morpho and Rvcg—shape analysis in R: R-packages for geometric morphometrics, shape analysis and surface manipulations. In Statistical Shape and Deformation Analysis, G. Zheng, S. Li, and G. Szelesky, eds. (Academic Press), pp. 217–256. https://doi.org/10.1016/B978-0-12-810493-4.00011-0.

60. Adams, D.C., and Otárola-Castillo, E. (2013). geomorph: an R package for the collection and analysis of geometric morphometric shape data. Methods Ecol. Evol. *4*, 393–399. https://doi.org/10.1111/2041-210X.12035.

61. Oksanen, J. (2020). vegan: Community Ecology Package. R package version 2.5–7. https://CRAN.R-project.org/package=vegan.

62. Revell, L.J. (2012). phytools: an R package for phylogenetic comparative biology (and other things). Methods Ecol. Evol. *3*, 217–223. https://doi.org/10.1111/j.2041-210X.2011.00169.x.

63. van der Meulen, A.J., García-Paredes, I., Álvarez-Sierra, M.Á., van den Hoek Ostende, L.W., Hordijk, K., Oliver, A., López-Guerrero, P., Hernández-Ballarín, V., and Peláez-Campomanes, P. (2011). Biostratigraphy or biochronology? Lessons from the Early and Middle Miocene small mammal events in Europe. Geobios *44*, 309–321. https://doi.org/10.1016/j.geobios.2010.11.004.

64. Rose, M.D., Leakey, M.G., Leakey, R.E.F., and Walker, A.C. (1992). Postcranial specimens of *Simiolus enjiessi* and other primitive catarrhines from the early Miocene of Lake Turkana, Kenya. J. Hum. Evol. *22*, 171–237. https://doi.org/10.1016/S0047-2484(05)80006-5.

65. Drake, R.E., Van Couvering, J.A., Pickford, M.H., Curtis, G.H., and Harris, J.A. (1988). New chronology for the Early Miocene mammalian faunas of Kisingiri, Western Kenya. J. Geol. Soc. *145*, 479–491. https://doi.org/10.1144/gsjgs.145.3.0479.

66. Senut, B. (1989). Le Coude des Primates Hominoïdes: Anatomie, Fonction, Taxonomie, Évolution (Editions du CRNS), p. 231.

67. Peppe, D.J., McNulty, K.P., Cote, S.M., Harcourt-Smith, W.E.H., Dunsworth, H.M., and Van Couvering, J.A. (2009). Stratigraphic interpretation of the Kulu Formation (Early Miocene, Rusinga Island, Kenya) and its implications for primate evolution. J. Hum. Evol. *56*, 447–461. https://doi.org/10.1016/j.jhevol.2009.02.006.

68. Pickford, M. (2007). A new suiform (Artiodactyla, Mammalia) from the early Miocene of East Africa. C. R. Palevol *6*, 221–229. https://doi.org/10.1016/j.crpv.2006.11.002.

69. Van Couvering, J.A., and Delson, E. (2020). African land mammal ages. J. Vertebr. Paleontol. *40*, e1803340. https://doi.org/10.1080/02724634.2020.1803340.

70. Russo, G.A., Prang, T.C., McGechie, F.R., Kuo, S., Ward, C.V., Feibel, C., and Nengo, I.O. (2024). An ape partial postcranial skeleton (KNM-NP 64631) from the Middle Miocene of Napudet, northern Kenya. J. Hum. Evol. *192*, 103519. https://doi.org/10.1016/j.jhevol.2024.103519.

71. Richmond, B.G., and Jungers, W.L. (1995). Size variation and sexual dimorphism in *Australopithecus afarensis* and living hominoids. J. Hum. Evol. *29*, 229–245. https://doi.org/10.1006/jhev.1995.1058.

72. Mitteroecker, P., and Bookstein, F. (2011). Linear discrimination, ordination, and the visualization of selection gradients in modern morphometrics. Evol. Biol. *38*, 100–114. https://doi.org/10.1007/s11692-011-9109-8.

73. Adams, D.C. (2014). A method for assessing phylogenetic least squares models for shape and other high-dimensional multivariate data. Evolution *68*, 2675–2688. https://doi.org/10.1111/evo.12463.

74. Zanolli, C., Bouchet, F., Fortuny, J., Bernardini, F., Tuniz, C., and Alba, D.M. (2023). A reassessment of the distinctiveness of dryopithecine genera from the Iberian Miocene based on enamel-dentine junction geometric morphometric analyses. J. Hum. Evol. *177*, 103326. https://doi.org/10.1016/j.jhevol.2023.103326.

75. Blomberg, S.P., Garland, T., Jr., and Ives, A.R. (2003). Testing for phylogenetic signal in comparative data: behavioral traits are more labile. Evolution *57*, 717–745. https://doi.org/10.1111/j.0014-3820.2003.tb00285.x.

76. Arnold, C., Matthews, L.J., and Nunn, C.L. (2010). The 10kTrees website: a new online resource for primate phylogeny. Evol. Anthropol. *19*, 114–118. https://doi.org/10.1002/evan.20251.

77. Monclús-Gonzalo, O., Alba, D.M., Duhamel, A., Fabre, A.-C., and Marigó, J. (2023). Early euprimates already had a diverse locomotor repertoire: Evidence from ankle bone morphology. J. Hum. Evol. *181*, 103395. https://doi.org/10.1016/j.jhevol.2023.103395.

78. Hunt, K.D., Cant, J.G.H., Gebo, D.L., Rose, M.D., Walker, S.E., and Youlatos, D. (1996). Standardized descriptions of primate locomotor and

postural modes. Primates *37*, 363–387. https://doi.org/10.1007/BF02381373.

79. Cramer, J.S. (2003). The origins and developments of the logit model. In Logit models from economics and other fields, J.S. Cramer, ed. (Cambridge University Press), pp. 149–158. https://doi.org/10.1017/CBO9780511615412.010.
80. Rohlf, F.J., and Corti, M. (2000). Use of two-block partial least-squares to study covariation in shape. Syst. Biol. *49*, 740–753. https://doi.org/10.1080/106351500750049806.
81. Wold, S., Trygg, J., Berglund, A., and Antti, H. (2001). Some recent developments in PLS modeling. Chemometr. Intell. Lab. Syst. *58*, 131–150. https://doi.org/10.1016/S0169-7439(01)00156-3.
82. Monclús-Gonzalo, O., Pal, S., Püschel, T.A., Urciuoli, A., Vinuesa, V., Robles, J.M., Almécija, S., and Alba, D.M. (2025). A dryopithecine talus from Abocador de Can Mata (Vallès-Penedès Basin, NE Iberian Peninsula): morphometric affinities and evolutionary implications for hominoid locomotion. Am. J. Biol. Anthropol. *186*, e70043. https://doi.org/10.1002/ajpa.70043.
83. Kuhn, M., and Johnson, K. (2013). Applied Predictive Modeling (Springer). https://doi.org/10.1007/978-1-4614-6849-3
84. Willmott, C.J., and Matsuura, K. (2005). Advantages of the mean absolute error (MAE) over the root mean square error (RMSE) in assessing average model performance. Clim. Res. *30*, 79–82. https://www.jstor.org/stable/24869236.

# STAR★METHODS

## KEY RESOURCES TABLE

| REAGENT or RESOURCE | SOURCE | IDENTIFIER |
|---|---|---|
| Deposited data | | |
| Raw landmark data of the complete sample used in the study | This study | https://doi.org/10.17632/dk7nhc9jjy.1 |
| 3D model of the radius of *Pliobates cataloniae* | This study/Institut Català de Paleontologia Miquel Crusafont | ark:/87602/m4/769006 |
| Comparative extant primate sample | This study (Table S8) | https://doi.org/10.17632/pp4bcpvv5n.1 |
| Software and algorithms | | |
| R | R Core Team[58] | https://www.r-project.org/ |
| Morpho package | Schlager[59] | https://cran.r-project.org/package=Morpho |
| Geomorph package | Adams and Otárola-Castillo[60] | https://cran.r-project.org/package=geomorph |
| vegan | Oksanen[61] | https://cran.r-project.org/package=vegan |
| Phytools | Revell[62] | https://cran.r-project.org/package=phytools |

## EXPERIMENTAL MODEL AND STUDY PARTICIPANT DETAILS

### Fossil sample

The studied specimen (IPS58443.16) is the left radius of a partial skeleton that constitutes the holotype of *P. cataloniae* and is housed at the Institut Català de Paleontologia Miquel Crusafont (ICP; Sabadell, Spain). The comparative fossil sample includes 10 radii (proximal and/or distal) of the following taxa (Table S7; Supplementary Methods): small-bodied stem catarrhines from East Africa, including *Simiolus enjiessi, Dendropithecus macinnesi*, *Micropithecus clarki*, and *Limnopitecus legetet*; African stem hominoids, including *Ekembo heseloni*, *Turkanapithecus kalakolensis*, and cf. *Rangwapithecus gordoni*; and the European pliopithecoid *Epipliopithecus vindobonensis*.

### Extant sample

The extant comparative sample includes 129 individuals from 22 genera (Table S8), encompassing extant hominoids, cercopithecoids, platyrrhines, and lorisids. Sex information was obtained from museum records and is reported in Table S8. Where possible, sex ratios within taxonomic groups were balanced; however, some specimens were listed as sex unknown, and preservation constraints limited the availability of comparable skeletal elements. Consequently, sex parity could not be fully maintained in all groups, with, e.g., platyrrhines biased toward males and hominoids toward females.

Because the study focuses on comparative skeletal morphology across broad taxonomic groups, sex was not included as a variable in statistical analyses. We therefore acknowledge that, while body mass effects on morphology were assessed, incorporating potential sex-related effects on morphology beyond body mass was not possible within the scope of this study.

## METHOD DETAILS

### Scanning methods

3D models of both extant and fossil radii were obtained with either a NextEngine surface laser scanner (NextEngine, Inc., Santa Monica) or microcomputed tomography (μCT) scanners (BIR ACTIS 225/300, Department of Human Evolution, Max Planck Institute for Evolutionary Anthropology, Leipzig, Germany; Nikon XT 225 ST, Cambridge Biotomography Center, Department of Zoology, University of Cambridge, Cambridge, UK; Nikon XTH 320, 3D Imaging Lab, Senckenberg Center for Human Evolution and Palaeoenvironment, Tübingen, Germany). Some 3D models of extant radii were downloaded from the MorphoSource repository (Table S8). Models done with the NextEngine scanner, which include the radius of *Pliobates* (scanned from the original fossil), were obtained using a resolution of >10,000 points per square inch; 6–12 scans were taken at two or more positions and then merged using ScanStudio HD PRO software v. 1.3.2 (Next Engine, Santa Monica). The isotropic voxel size for the μCT scans sample ranges from 21.9 to 51.5 μm. Laser scan-derived 3D models were cleaned (fill holes, irregularities in mesh, etc.) using Geomagic Wrap 2017 (3D Systems, Inc. Morrisville), and μCT scans were processed in AVIZO v. 6.3 (Visualization Sciences Group, Berlin). All 3D models of fossil specimens were obtained from the original fossils except for *Simiolus* and *Epipliopithecus*, which were scanned from research quality casts housed in the ICP.

### Fossil dates

The fossils in the sample (Table S7) have the following age estimates: (1) *E. vindobonensis*, 14.15 Ma (average of the maximum and minimum age ranges for MN6 in central Europe)[63] (2) *S. enjiessi*, 17.2 Ma (average of the ages of Kalodirr [16.7 Ma] and Moruorot [17.7 Ma])[64]; (3) *D. macinnesi*, 17.8 Ma (age of locality R3a from the Hiwegi Formation of Rusinga Island)[65–67]; (4) *Micropithecus clarki*, 20.3 Ma (age of the Chamtwara member)[68]; (5) cf. *Rangwapithecus gordoni*, 20.3 Ma (age of the Songhor locality)[69]; (6) *Limnopithecus legetet*, 20.3 Ma (age of Koru formation)[69]; (7) *Ek. heseloni*, 17.8 Ma (age of the Kulu Formation of Rusinga Island)[67]; and (8) *Turkanapithecus kalakolensis*, 17.5 Ma (age of the Kalodirr locality).[28,69] Note that cf. *R. gordoni* corresponds to KNM-SO 1009 from Songhor, generally attributed tentatively to this species[39,68] but potentially also attributable to *Proconsul africanus*,[66,70] which is also recorded there.

## QUANTIFICATION AND STATISTICAL ANALYSIS

### Landmark protocols

The morphometric affinities of IPS58443.16 were assessed using 3D surface landmarks, using three different protocols. For the proximal epiphysis, the protocol was based on previous works[12,42] but landmarks were added, particularly to the posterior aspect of the radial head, previously unexplored. For the distal epiphysis and the whole radius (Figure S10 and Table S9), new landmark protocols were devised, partially based on previous works on the same structures (e.g., Tallman[44]). Different protocols were used to independently assess the shape variation of each epiphysis, which according to previous studies are highly functionally informative.[12,42] Moreover, for whole bone analysis most of the variance corresponds to the relative size between the diaphysis and the epiphyses (i.e., to the overall robustness of the bone[71]), which may easily lead to overlooking important details from the joints. As such, the proximal radius protocol consists of 17 landmarks (Table S9 and Figure S10) and used the landmarks of the proximal epiphysis of complete radius protocol with added landmarks from previous protocols used by the authors.[12,42] The protocol captures the most informative elements of the radial head, including the shape of the fovea, the articular surface (e.g., presence/absence of bevel), and radial neck length. For the placing of type II landmarks (dependent on orientation on one of their coordinates), the complete radii were anatomically oriented in anterior view, which readily allowed the identification of the medial, lateral, and posterior aspects of the radial head. The protocol for the distal radius involved the landmarks from the initial complete radius protocol corresponding to the distal epiphysis and consisted of 15 landmarks (Table S9 and Figure S10). The complete radius protocol consisted of 36 landmarks distributed throughout the radius, and recorded all the key homologous points of the bone, such as the shape of the radial head, the length and curvature of the diaphysis and the key anatomical elements of the distal epiphysis (e.g., styloid length and position; Table S9 and Figure S10).

### 3D geometric morphometric analyses

The landmark 3D coordinates, for each protocol separately, were translated, rotated, and size-scaled to unit centroid size (CS) using a generalized Procrustes analysis (GPA) with the "Morpho" v. 2.8 package[59] in R v. 3.6.1.[58] We performed a between-group principal component analysis (bgPCA)[72] on the GPA-transformed coordinates of the extant sample, with major anthropoid clades (platyrrhines, cercopithecoids, hominoids) and lorisids as *a priori* defined groups. Such broad taxonomic groups were used to ascertain morphological (not phylogenetic) affinities. The fossil configurations were projected a posteriori onto the morphospace generated by the bgPCA. To rule out the presence of spurious grouping in the sample, we computed a cross-validated bgPCA (cv-bgPCA) and compared the results to those of the standard bgPCA. Additionally, group mean differences were tested with a permutational analysis of variance (PERMANOVA; 1000 permutations) based on the Euclidean distances between the means. We computed the Z scores and the $R^2$ (i.e., the amount of variance explained) for group differences in the raw shape data, and the scores of both the standard and the cv-bgPCAs using the "vegan" v. 2.5 package[61] in R. The correlation between bgPC scores and log-transformed CS (with natural logarithms, ln) was computed by means of a phylogenetic generalized least squares (PGLS) regression[73] using the "geomorph" v. 3.1.1 package[60] in R. We additionally performed PCAs on the three datasets to check for similarity without *a priori* assumptions in group distribution with respect to the bgPC analyses. We further performed canonical variate analysis (CVA) without and with cross-validation for all datasets with the same broad *a priori* groups as for the bgPCA. We ran the CVA on a subset of PC scores that maximized the percentage of correct classification with the minimum number of PCs[74]; following this procedure, we selected 8 PCs for the distal dataset, 11 for the proximal and 9 for the whole radius, obtaining 94% correct classification, 86% and 95% respectively (Figure S11). We computed posterior and typicality probabilities to classify the fossils into the *a priori* groups. Posterior probabilities in CVA reflect the relative likelihood of group membership with values adding up to 1 across all groups; on the other hand, typicality probabilities reflect how well a specimen fits within the distribution of each group separately and are expressed as *p* values.

We calculated the phylogenetic signal for the three datasets (both with and without fossils) to assess the amount of homoplasy (or lack thereof) embedded in radial shape by means of Blomberg's K[75] using the "phytools" v. 0.6–60 package[62] in R. $K = 0$ implies a model of evolution that closely resembles that expected under Brownian motion. Blomberg's *K* tests the null hypothesis of no phylogenetic signal (i.e., closely related species do not resemble each other more than distant relatives) by comparing the observed data distribution to that expected under a Brownian motion model of evolution. It informs about how well the distribution of the phylogenetic tree tips reflects the patterns of variance-covariance found in the data.[75] For $K < 1$, the variance accumulates within the clades,

with closely related taxa resembling each other less than expected, possibly as a consequence of independent evolution (i.e., homoplasy). Finally, when $K > 1$, non-closely related taxa are more similar than expected under a Brownian motion model of evolution, implying the variance accumulates among clades, as the result of stabilizing selection or architectural constraints. For the extant taxa, we relied on a molecular-based time-calibrated phylogenetic tree downloaded from 10kTrees website v. 3[76] (Figure S12A). The extinct taxa were added according to their phylogenetic relationships (Figures S12B–S12D) as inferred by recent cladistic studies.[1,7,31] The divergence time of the nodes for extinct taxa was arbitrarily set 1 Myr prior to the divergence of the next derived node. The tip age estimates used for the fossils are described above.

### Locomotor frequency analysis

A quantitative dataset of locomotor percentages was compiled from the literature for all taxa included in the extant comparative sample. The following locomotor types were distinguished: quadrupedalism (Q), leaping (L), FDS, climbing (CLI), and clambering (CLA). Following Monclús-Gonzalo et al.,[77] the locomotor behavior percentages used in this study were compiled from the literature (Table S10). To standardize the data and minimize discrepancies arising from different categories used in different field studies, we established the percentages by selecting a minimum number of distinct sources (in total, 18 references were used). We then organized the data into five broad locomotor types based on the standardized primate locomotor modes described by Hunt et al.[78]

1. Quadrupedalism: This mode includes both arboreal and terrestrial quadrupedalism on supports of varying sizes and angles. The torso is oriented roughly parallel to the substrate (pronogrady), and the gait is symmetrical. It comprises ''quadrupedal walking'', ''quadrupedal running'', ''galloping'', and ''bounding''.
2. Leaping: It refers to behaviors characterized by an extended period of free flight followed by a precise landing on a second support. This category includes ''leaping'', ''vertical leaping'', ''hopping'', and ''dropping''.
3. Forelimb-dominated suspension: This mode includes any locomotor behavior where at least one forelimb is under tension, carrying body weight. It includes ''arm swinging'', ''brachiation'', ''bimanual suspension'', and ''swaying''.
4. Climbing: It is the progression on supports angled at more than 45°, typically engaging all four limbs in an irregular pattern, and is characterized by diverse hand and foot movements and positions. It comprises ''climbing'', ''vertical descent'', and ''cantilevering''.
5. Clambering: It is defined as a non-suspensory form of progression with an irregular gait. This type includes ''clambering'' and ''scrambling''.

A logit transformation was applied to the locomotor data, a standard technique to extend infinitely the bounds of an originally limited distribution (e.g., proportions) and thus avoid unexpected results when conventional parametric statistical methods are applied.[79] Values of 0% were corrected by adding 1% prior to transformation.

A type of partial least-squares analysis,[80] known as partial least-squares regression, was used to examine the covariation between radial shape (for the proximal, distal, and complete radius) and locomotor percentages (Table S10). This analysis enables the generation of predictive models[81] and has been employed to predict the locomotor behavior of extinct primates.[77,82] To assess the predictive performance of the PLSR, a leave-one-out cross-validation was conducted.[83] Later, the mean absolute error (MAE; i.e., the arithmetic average of the absolute errors) was calculated from the cross-validated results to evaluate the accuracy of locomotor mode predictions within the extant sample.[84] Then, to obtain the locomotor predictions, radial shape values for extinct species were projected onto the latent space generated after the 2B-PLS and then multiplied by a matrix consisting of the linear model coefficients calculated after the regression of the first block of variables on the scores for the second block. After that, the obtained latent variables were transformed back into percentages by applying an inverse logit transformation, defined as exp(X)/[1 þ exp(X)], where X corresponds to a logit-transformed value. The obtained predictions were then rounded up again to ensure that they added up to 100%. Humans were excluded from the PLSR as we did not consider bipedalism in the analyses as a locomotor type. We then performed the locomotor frequency analyses, both including and excluding African apes (gorillas and chimpanzees). We excluded them because their modern-ape-like radial shape, coupled with their high percentage of quadrupedalism (Table S10), had a large confounding effect on the analysis.

## ADDITIONAL RESOURCES

### Morphosource

Description: URL. 3D models, X-ray (micro)tomography, and derived data repository. https://morphosource.org/.